Inorg. Chem. **2009**, *48*, 3916−3925

Structure Modulated Electronic Contributions to Metalloenediyne Reactivity: Synthesis and Thermal Bergman Cyclization of MLX_2 Compounds

Sibaprasad Bhattacharyya, Aurora E. Clark, Maren Pink, and Jeffrey M. Zaleski*

Department of Chemistry and Molecular Structure Center, Indiana University, Bloomington, Indiana 47405

Received June 17, 2008

The synthesis of novel metalloendiyne complexes $MLRX_2$ (where L = 1,4-dibenzyl/diethyl-1,4-diaza-cyclododec-8-ene-6,10-diyne, X = halogen) are reported with their X-ray crystal structures and thermal Bergman cyclization temperatures. Two distinct types of constructs are obtained; the Zn(II) compounds are tetrahedral, while the Cu(II) and the Pd(II) compounds are all distorted- or square-planar. Each possesses structurally similar enediyne conformations and critical distances (3.75−3.88 Å). The tetragonal Cu(II) species all exhibit Bergman cyclization temperatures between 140 and 150 °C in the solid state, while the square-planar Pd(II) analogues possess similar critical distances but cyclize at significantly higher temperatures (205−220 °C). In contrast, the Zn(II) derivatives show a marked halogen dependence, with X = Cl having the highest Bergman cyclization temperature, which is comparable to the Pd(II) square-planar set, while the $ZnLX_2$ compound with X = I shows the lowest Bergman cyclization temperature (144 °C), similar to the Cu(II) derivatives. Moreover, for the planar constructs, the R group has little influence on the cyclization temperatures; however, for the tetrahedral $ZnLX_2$ compounds, the steric influence of the R group plays a more significant role in the cyclization reaction coordinate by influencing the stability of the precyclized intermediate. This complex set of results is best interpreted by a combination of steric contributions and electronic interactions between the halogen through space (in the case of Zn(II)) and through bonds (in the case of Pd(II)) and the π orbitals of the endiyne fragment. In contrast, for Cu(II) systems, the distorted square-planar geometry permits neither direct through space nor symmetry-allowed through bond communication between the orbital partners, and thus little variation in Bergman cyclization reactivity is observed.

Introduction

The reactivities of metal-bound substrates are dependent upon the geometric and electronic properties of the metal cofactor. This is evident in bioinorganic chemistry, organometallic transformations, and polymerization catalysis. The thermal and photochemical reactivities of enediyne ligands coordinated to metal cofactors are no different in that the metal-center geometric and electronic properties can modulate the thermal or photochemical reactivities of the bound enediyne.[1−8] This is especially true when metal properties are judiciously chosen to complement the conformational flexibility of the enediyne ligand, or the electron-donating or -accepting properties of the metal-binding functionalities. Although tunability in reactivity via the metal oxidation state, intraligand electronic properties, and even ancillary ligand influences (geometric and electronic) is expected, it becomes challenging to independently isolate the contributions from each of these components within a discrete set of molecules.

* Author to whom correspondence should be addressed. E-mail: zaleski@indiana.edu.

(1) Bhattacharyya, S.; Dye, D. F.; Pink, M.; Zaleski, J. M. *Chem. Commun.* **2005**, 5295–5297.
(2) Bhattacharyya, S.; Pink, M.; Baik, M.-H.; Zaleski, J. M. *Angew. Chem., Int. Ed.* **2005**, *44*, 592–595.
(3) Bhattacharyya, S.; Pink, M.; Huffman, J. C.; Zaleski, J. M. *Polyhedron* **2006**, *25*, 550–558.
(4) Bhattacharyya, S.; Zaleski, J. M. *Curr. Top. Med. Chem.* **2004**, *4*, 1637–1654.
(5) O'Connor, J. M.; Friese, S. J.; Rodgers, B. L. *J. Am. Chem. Soc.* **2005**, *127*, 16342–16343.
(6) O'Connor, J. M.; Friese, S. J.; Tichenor, M. *J. Am. Chem. Soc.* **2002**, *124*, 3506–3507.
(7) O'Connor, J. M.; Lee, L. I.; Gantzel, P.; Rheingold, A. L.; Lam, K.-C. *J. Am. Chem. Soc.* **2000**, *122*, 12057–12058.
(8) Rawat, D. S.; Zaleski, J. M. *Synlett* **2004**, 393–421.

10.1021/ic801116q CCC: $40.75
Published on Web 08/30/2008

In a preliminary communication, we showed a unique effect in metal-modulated enediyne reactivity. By preparing a conformationally restricted enediyne based on the 1,4-dibenzyl-1,4-diaza-cyclododec-8-ene-6,10-diyne scaffold, and chelating this ligand to Zn(II) and Cu(II) dihalogen fragments, we are able to obtain structurally similar enediyne conformations with markedly different geometric structures at the metal center.[9] This is due to the ethylenediamine bridge, which inhibits the enediyne ligand from responding to the metal-mandated geometric structural change. The result is a series of coordination compounds with either distorted square-planar (in the case of Cu(II)) or tetrahedral (in the case of Zn(II)) geometries with near-identical enediyne conformations and critical distances (on the order of 3.8 Å). Although this suite of molecules possesses similar enediyne dispositions, their thermal reactivities vary by ∼70 °C. A preliminary density functional theory calculation suggested a structure-dependent electronic effect involving the halogen ancillary ligands that was leading to the observed reactivity. However, several questions remained unanswered. What is the magnitude and range of this effect in terms of thermal cyclization reactivity? How does it vary with halogen and metal-halogen bond length? From a more mechanistic perspective, what specifically is the nature of the halogen interaction with the enediyne? Is the ground state stabilized or is the transition state destabilized? How dependent is this effect on the metal-ancillary ligand fragment? Does the R group on the enediyne play any role whatsoever or is it a spectator functionality?

To address these questions, we have broadened the subset of MLX_2 compounds to include the square-planar d^8 Pd(II) systems as well as the series X = Cl, Br, and I. In addition, we have prepared a complementary enediyne ligand where the R group (R = phenyl) of the coordinating amine has been substituted with the less-sterically cumbersome methyl group (R = Me; L = 1,4-diethyl-1,4-diaza-cyclododec-8-ene-6,10-diyne). Several of these compounds have been crystallographically characterized, and their Bergman cyclization temperatures have been evaluated using a combination of NMR and differential scanning calorimetry (DSC). This family of structures allows the systematic evaluation of the electronic influences of the halogen within a series of geometrically modulated and sterically distinct complexes. Combined with the conclusions drawn from a density functional study of the thermal Bergman cyclization reaction coordinates for these constructs,[10] the results suggest that indeed there is a very subtle interplay between the geometric structure of the corresponding metal center, the identity of the halogen, and the overall electronic structure of the complexes. More subtly, the steric influences of the R group also play a meaningful role in affecting the Bergman cyclization reaction coordinate.

(9) Bhattacharyya, S.; Clark, A. E.; Pink, M.; Zaleski, J. M. *Chem. Commun.* **2003**, 1156–1157.
(10) Clark, A. E.; Bhattacharyya, S.; Pink, M.; Zaleski, J. M. *Inorg. Chem.* **2008**, 3926-3933.

Experimental Methods

Materials. 1,8-Dibromooct-4-ene-2,6-diyne was prepared according to a literature method.[11,12] Reactions were carried out under nitrogen using Schlenk and drybox techniques. Hydrocarbon solvents such as diethyl ether and benzene were dried by distillation over sodium/benzophenone prior to use. Methylene chloride and *n*-butylamine were dried over calcium hydride and distilled. Organic enediynes were purified by flash chromatography using silica gel (200−440 mesh). All other chemicals and solvents were used as received from Aldrich, Strem, and Fluka.

Physical Measurements. ^{1}H NMR and ^{13}C NMR spectra were recorded on a VXR 400 NMR spectrometer using the residual proton resonance of the solvent as an internal reference. Infrared spectra were recorded on a Nicolet 510P FTIR spectrometer. Elemental analyses on all samples were obtained from Robertson Microlit Laboratories Inc., and mass spectral data were obtained at the University of Illinois with a micromass Quatto-I mass spectrometer. Electronic absorption spectra were obtained on a Perkin-Elmer Lambda 19 UV/vis/near-IR spectrometer. DSC traces were measured on a V4.1 Dupont 910 DSC differential scanning calorimeter coupled to a Dupont thermal analyst 2100 at a heating rate of 10 °C min^{-1}.

Syntheses. Ligands LR (R = Ph, 1a) and LR′ (R′ = Me, 1a′). The same general methods have been used for the preparations of ligands **1a** and **1a′**. The synthesis of compound **1a** has been previously reported,[9] while that of **1a′** is described below.

1,4-Ethyl-1,4-diaza-cyclododec-8-ene-6,10-diyne (LMe, 1a′). A flask was charged with N,N′-diethylethylenediamine (1 g, 8.6 mmol) and anhydrous potassium carbonate (4.0 g, 28.9 mmol) in dry dimethylformamide (30 mL), and the mixture was allowed to stir at 0 °C for 10 min. A solution of 1,8-dibromooct-4-ene-2,6-diyne (2.25 g, 8.6 mmol) in dry dimethylformamide (20 mL) was then added dropwise over 1 h. The reaction mixture was allowed to stir for 3 h at 0 °C. After completion of the reaction, the solid was filtered and washed with dimethylformamide (2 × 10 mL). The combined organic layers were poured into water (300 mL) and then extracted with methylene chloride (50 mL). The methylene chloride layer was washed with water (3 × 200 mL) and dried over anhydrous sodium sulfate. Finally, the solvent was removed under reduced pressure. The crude product was purified on a silica gel column with 10% methanol in dichloromethane as the eluent. Yield: 400 mg (22%); white solid. ^{1}H NMR (400 MHz, $CDCl_3$): δ 5.80 (s, 2H), 3.50 (s, 4H), 2.83 (s, 4H), 2.52 (m, 4H), 1.06 (t, 6H). ^{13}C NMR (400 MHz, $CDCl_3$): δ 121.35 (CH), 93.53 (Cquat), 83.76 (Cquat), 51.59 (CH_2), 50.70 (CH_2), 43.83 (CH_2), 12.83 (CH_3). IR (KBr, cm^{-1}): 3036, 2965, 2855, 2196, 1730, 1474, 1445, 1330, 1336, 1223, 1075, 920, 774, 547. MS (EI): *m/z* 216 (M^+). Anal. calcd for $C_{14}H_{20}N_2$: C, 77.73; H, 9.32; N, 12.95. Found: C, 77.66; H, 9.37; N, 13.10.

Dihalo-(1,4-dibenzyl/diethyl-1,4-diaza-cyclododec-8-ene-6,10-diyne)copper(II) (2a−2b). A 50 mL round-bottom flask was charged with $CuCl_2 \cdot 2H_2O$/$CuBr_2$ (0.35 mmol), which was then dissolved in reagent-grade methanol (5 mL). A solution of ligand LPh/LMe (0.35 mmol) in methylene chloride (5 mL) was then added dropwise. The mixture was allowed to stir for 3 h, after which a precipitate formed. The product was further precipitated by the addition of diethylether (20 mL). The solid product was then filtered and dried under a vacuum overnight. Yield: 90%. **Cu(LMe)Cl_2 (2a′).** IR (KBr, cm^{-1}): 3125, 2945, 2840, 1570, 1484,

(11) König, B.; Pitsch, W.; Dix, I.; Jones, P. G. *Synthesis* **1996**, 446–448.
(12) Benites, P. J.; Rawat, D. S.; Zaleski, J. M. *J. Am. Chem. Soc.* **2000**, *122*, 7208–7217.

Table 1. Selected Bond Lengths (Å) and Angles (deg) of **2a′** and **2b**

2a′		**2b**	
	Distance		
Cu1A−N1A	2.061(2)	Cu1−N1	2.0822(18)
Cu1A−N2A	2.097(2)	Cu1−N2	2.0980(18)
Cu1A−Cl1A	2.2479(7)	Cu1−Br2	2.3671(4)
Cu1A−Cl2A	2.2530(7)	Cu1−Br1	2.4052(4)
C2A−C3A	1.186(4)	C2−C3	1.195(3)
C4A−C5A	1.335(4)	C4−C5	1.336(3)
C6A−C7A	1.192(4)	C6−C7	1.19
	Angles		
N1A−Cu1A−N2A	84.65(8)	N1−Cu1−N2	85.18(7)
N1A−Cu1A−Cl1A	91.45(6)	N1−Cu1−Br2	166.17(5)
N2A−Cu1A−Cl1A	170.42(6)	N2−Cu1−Br2	92.16(5)
N1A−Cu1A−Cl2A	176.08(6)	N1−Cu1−Br1	92.84(5)
N2A−Cu1A−Cl2A	91.44(6)	N2−Cu1−Br1	170.60(5)
Cl1A−Cu1A−Cl2A	92.36(2)	Br2−Cu1−Br1	91.890(13)

1360, 1202, 1018, 910, 753, 721. Anal. calcd for $C_{14}H_{20}N_2Cl_2Cu$: C, 47.94; H, 5.75; N, 7.99. Found: C, 48.12; H, 5.83; N, 7.87. **Cu(LPh)Br$_2$ (2b).** IR (KBr, cm^{-1}): 3120, 2953, 2842, 1558, 1490, 1340, 1207, 1025, 910, 750, 711. Anal. calcd for $C_{24}H_{24}N_2Br_2Cu$: C, 51.13; H, 4.29; N, 4.97. Found: C, 51.23; H, 4.13; N, 5.11.

Dihalo-(1,4-dibenzyl/diethyl-1,4-diaza-cyclododec-8-ene-6,10-diyne)zinc(II) (3a−3c). The same general methods have been used for the preparation of **3a−3c**. For Zn(LPh)Br$_2$ (**3b**), a 50 mL Schlenk flask was charged with $ZnBr_2$ (78 mg, 0.35 mmol), which was then dissolved in dry methanol (5 mL). Ligand **1a** (119 mg, 0.35 mmol) in methylene chloride (5 mL) was added dropwise, and the solution was stirred for 3 h under nitrogen. The colorless solution was then evaporated to dryness under a vacuum. The white product was subsequently extracted with methylene chloride and filtered. Slow evaporation of the filtrate afforded **3b**. Yield: 134 mg (70%). **Zn(LMe)Cl$_2$ (3a′).** ^{1}H NMR (400 MHz, CD_2Cl_2): δ 5.92 (s, 2H), 4.11 (s, 4H), 3.44 (s, 4H), 2.81 (s, 4H), 1.26 (s, 6H). IR (KBr, cm^{-1}): 3011, 2945, 2795, 1582, 1440, 1352, 1208, 1011, 910, 711. Anal. calcd for $C_{14}H_{20}N_2Cl_2Zn$: C, 47.69; H, 5.72; N, 7.94. Found: C, 47.76; H, 5.81; N, 8.16. **Zn(LPh)Br$_2$ (3b).** ^{1}H NMR (400 MHz, CD_2Cl_2): δ 7.43 (d, 4H), 7.37−7.34 (m, 6H), 5.92 (s, 2H), 4.15 (s, 4H), 3.82 (s, 4H), 3.52 (s, 4H). IR (KBr, cm^{-1}): 3020, 2940, 2780, 1560, 1445, 1361, 1205, 1017, 945, 728, 712. Anal. calcd for $C_{24}H_{24}N_2Br_2Zn$: C, 50.96; H, 4.28; N, 4.95. Found: C, 51.15; H, 4.39; N, 4.87. **Zn(LMe)Br$_2$ (3b′).** ^{1}H NMR (400 MHz, CD_2Cl_2): δ 5.91 (s, 2H), 4.14 (s, 4H), 3.40 (s, 4H), 2.92 (s, 4H), 1.36 (s, 6H). Anal. calcd for $C_{14}H_{20}N_2Br_2Zn$: C, 38.08; H, 4.56; N, 6.34. Found: C, 37.88; H, 4.72; N, 6.22. **Zn(LPh)I$_2$ (3c).** ^{1}H NMR (400 MHz, CD_2Cl_2): δ 7.42 (d, 4H), 7.39−7.34 (m, 6H), 5.89 (s, 2H), 4.22 (s, 4H), 3.77 (s, 4H), 3.45 (s, 4H). ^{13}C NMR (400 MHz, $CDCl_3$): δ 132.56, 131.22, 129.30, 128.16, 121.57, 90.93, 87.54, 62.26, 50.90, 45.58. IR (KBr, cm^{-1}): 3010, 2940, 2795, 1580, 1445, 1356, 1205, 1017, 945, 728, 712. Anal. calcd for $C_{24}H_{24}N_2I_2Zn$: C, 43.70; H, 3.67; N, 4.25. Found: C, 43.58; H, 3.54; N, 4.11. **Zn(LMe)I$_2$ (3c′).** ^{1}H NMR (400 MHz, CD_2Cl_2): δ 5.87 (s, 2H), 4.06 (s, 4H), 3.46 (s, 4H), 2.84 (s, 4H), 1.28 (s, 6H). Anal. calcd for $C_{14}H_{20}N_2I_2Zn$: C, 31.40; H, 3.76; N, 5.23. Found: C, 31.16; H, 3.58; N, 5.38.

Dichloro-(1,4-dibenzyl/diethyl-1,4-diaza-cyclododec-8-ene-6,10-diyne)palladium(II) (4a−4a′). The same general procedures have been used for the syntheses of complexes **4a** and **4a′**. For Pd(LPh)Cl$_2$ (**4a**), a solution of ligand **1a** (41 mg, 0.12 mmol) in methylene chloride (25 mL) was added to a stirring solution of bis(acetonitrile)palladium(II)chloride (39 mg, 0.15 mmol) in methylene chloride (20 mL) under nitrogen. The mixture was allowed to stir at room temperature for 2 h. The solvent was evaporated, and the residue was purified on silica gel with methylene chloride/methanol (100:1) as the eluent. Evaporation of the solvent afforded **4a**. Yield: 44 mg (70%). ^{1}H NMR (400 MHz, CD_2Cl_2): δ 7.65 (d, 4H), 7.48−7.41 (m, 6H), 5.96 (s, 2H), 4.62 (d, 2H), 3.92 (d, 2H), 3.65 (t, 2H), 3.61 (d, 2H), 3.07 (d, 2H), 2.98 (t, 2H). ^{13}C NMR (400 MHz, CD_2Cl_2): δ 132.95 (Cquat), 131.14 (CH), 130.03 (CH), 129.32 (CH), 121.29 (CH), 92.17 (Cquat), 87.47 (Cquat), 63.65 (CH_2), 56.03 (CH_2), 52.65 (CH_2). UV−vis (λ_{max}, nm (ε, M^{-1}cm^{-1})): 395(270), 235(24 240). IR (KBr, cm^{-1}): 3054, 2920, 2204, 1652, 1454, 1350, 1204, 1018, 927, 737, 705. Anal. calcd for $C_{24}H_{24}N_2Cl_2Pd$: C, 55.67; H, 4.67; N, 5.41. Found: C, 55.77; H, 4.90; N, 5.25. **Pd(LMe)Cl$_2$ (4a′).** ^{1}H NMR (400 MHz, CD_2Cl_2): δ 6.06 (s, 2H), 4.38 (d, 2H), 3.79 (d, 2H), 3.28 (t, 2H), 3.16 (d, 2H), 3.09 (d, 2H), 2.83 (t, 2H), 1.44 (t, 6H). ^{13}C NMR (400 MHz, CD_2Cl_2): δ 121.29, 92.04, 87.68, 57.28, 56.35, 52.03, 10.39. IR (KBr, cm^{-1}): 3020, 2925, 2210, 1731, 1453, 1342, 1261, 1101, 1026, 800, 758. Anal. calcd for $C_{14}H_{20}N_2Cl_2Pd$: C, 42.72; H, 5.12; N, 7.12. Found: C, 42.77; H, 4.97; N, 7.25.

Scheme 1. Syntheses of Cyclic Enediyne Ligands **1**

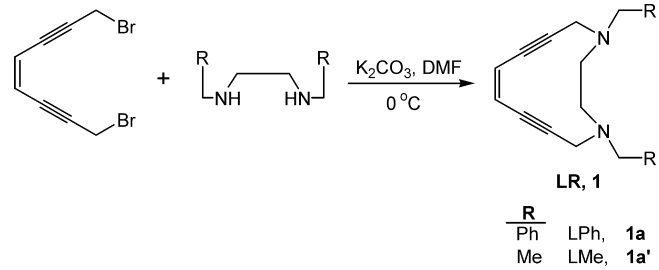

Dibromo-(1,4-dibenzyl-1,4-diaza-cyclododec-8-ene-6,10-diyne)-palladium(II) (4b). A solution of ligand **1a** (41 mg, 0.12 mmol) in methylene chloride (25 mL) was added to a stirring solution of palladium(II) dibromide (39 mg, 0.15 mmol) in methylene chloride (10 mL) under nitrogen. The mixture was allowed to stir at room temperature for 24 h. The solvent was evaporated, and the residue was repeatedly washed with diethyl ether, which afforded **4b** as an air-stable brown solid. Yield: 64 mg (80%). ^{1}H NMR (400 MHz, CD_2Cl_2): δ 7.64 (d, 4H), 7.45−7.41 (m, 6H), 5.97 (s, 2H), 4.80 (d, 2H), 3.99 (d, 2H), 3.72 (d, 2H), 3.66 (t, 2H), 3.23 (d, 2H), 2.98 (t, 2H). UV−vis (λ_{max}, nm (ε, M^{-1}cm^{-1})): 365(1220), 251(33 130). IR (KBr, cm^{-1}) 3055, 2921, 2204, 1673, 1453, 1350, 1205, 1018, 922, 730, 701. Anal. calcd for $C_{24}H_{24}N_2Br_2Pd$: C, 47.51; H, 3.99; N, 4.62. Found: C, 47.77; H, 4.20; N, 4.45.

Diiodo-(1,4-dibenzyl-1,4-diaza-cyclododec-8-ene-6,10-diyne)-palladium(II) (4c). A solution of ligand **1a** (62 mg, 0.18 mmol) in dry tetrahydrofuran (THF; 5 mL) was added to a stirring solution of palladium(II) acetate (41 mg, 0.18 mmol) and sodium iodide (123 mg, 0.82 mmol) in dry THF (5 mL) under nitrogen. The mixture was allowed to reflux for 24 h. The solvent was evaporated, and the residue was purified on silica gel with methylene chloride/methanol (100:1) as the eluent. Evaporation of the solvent afforded **4c**. Yield: 50 mg (40%). ^{1}H NMR (400 MHz, CD_2Cl_2): δ 7.57 (d, 4H), 7.42−7.38 (m, 6H), 5.96 (s, 2H), 4.88 (d, 2H), 3.98 (d, 2H), 3.83 (t, 2H), 3.60 (d, 2H), 3.48 (d, 2H), 2.89 (t, 2H). UV−vis (λ_{max}, nm (ε, M^{-1}cm^{-1})): 500(1295), 267(18 910). IR (KBr, cm^{-1}): 3031, 2921, 2204, 1673, 1453, 1350, 1205, 1018, 925, 737, 703. Anal. calcd for $C_{24}H_{24}N_2I_2Pd$: C, 41.12; H, 3.45; N, 4.01. Found: C, 41.21; H, 3.55; N, 4.20.

Characterization of Thermal Product (5) Derived from 1a′. A Schlenk flask was charged with 50 mg of **1a′**, and a 100-fold excess of 1,4-cyclohexadiene was added in 5 mL of dimethylsulfoxide (DMSO). The mixture was heated to 170 °C for 10 h. The solution turned to dark brown upon heating. The product was extracted with methylene chloride and was washed several times

Scheme 2. Syntheses of Cu(II) Enediyne Dihalide Complexes **2**−**2b**

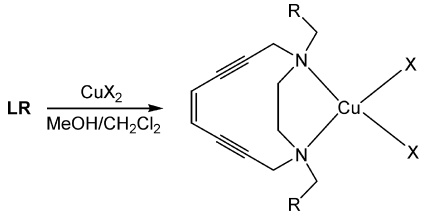

2

R	X		
Ph	Cl	$Cu(LPh)Cl_2$,	**2a**
Me	Cl	$Cu(LMe)Cl_2$,	**2a'**
Ph	Br	$Cu(LPh)Br_2$,	**2b**

Scheme 3. Syntheses of Zn(II) Enediyne Dihalide Complexes **3**−**3c**

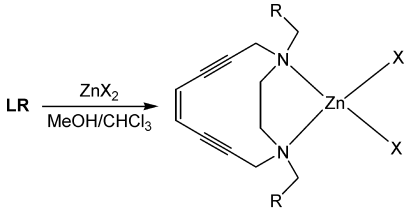

3

R	X		
Ph	Cl	$Zn(LPh)Cl_2$,	**3a**
Ph	Br	$Zn(LPh)Br_2$,	**3b**
Ph	I	$Zn(LPh)I_2$,	**3c**
Me	Cl	$Zn(LMe)Cl_2$,	**3a'**
Me	Br	$Zn(LMe)Br_2$,	**3b'**
Me	I	$Zn(LMe)I_2$,	**3c'**

with water using a separating funnel. The organic layer was dried with Na_2SO_4 and the solvent removed under a vacuum. A dark brown oil was obtained and purified by flash chromatography (5% $MeOH/CH_2Cl_2$), yielding a pale yellow solid. Yield: 28 mg (56%). ^1H NMR (400 MHz, $CDCl_3$): δ 7.19 (m, 4H), 3.98 (s, 4H), 2.74 (s, 4H), 2.56 (m, 4H), 1.17 (t, 6H). ^{13}C NMR (400 MHz, $CDCl_3$): δ 136.06, 130.78, 127.08, 54.29, 49.59, 48.82, 12.87. MS (EI): *m*/*z* 218 (M^+). Anal. calcd for $C_{14}H_{22}N_2$: C, 77.02; H, 10.16; N, 12.83. Found: C, 77.11; H, 10.39; N, 12.61.

Isolation of Thermal Product (5) Derived from 2a′. A Schlenk flask was charged with 100 mg of **2**, and a 100-fold excess of 1,4-cyclohexadiene was added in 5 mL of DMSO. The mixture was heated to 140 °C for 6 h. The green solution turned to dark brown upon heating. After cooling, 2.2 equiv of silver nitrate dissolved in acetonitrile was added. The solution was stirred for 4 h at room temperature. An aqueous suspension of excess ethylenediaminetetraacetic acid (EDTA; 10-fold) was then added, and the solution was allowed to stir overnight. The precipitate formed was filtered, and the filtrate was kept to extract the organic thermal product. The organic product was extracted with methylene chloride and washed several times with water. The organic layer was dried with Na_2SO_4 and the solvent removed in vacuo. A dark brown oil was obtained and purified by flash chromatography (5% $MeOH/CH_2Cl_2$), yielding a yellow solid. Yield: 18 mg (25%).

X-Ray Structure Determination. X-ray-quality crystals of **2a′**, **2b**, **3b**, **3c′**, **3d**, and **4a**−**4c** were grown by the slow diffusion of hexane in dichloromethane at 0 °C. In all cases, a suitable crystal was placed onto the tip of a 0.1-mm-diameter glass capillary and mounted on a SMART6000 (Bruker) at 120 K. A preliminary set of cell constants was calculated from reflections harvested from three sets of 20 frames. These initial sets of frames were oriented such that orthogonal wedges of reciprocal space were surveyed.

Scheme 4. Syntheses of Pd(II) Enediyne Dichloride Complexes **4** and **4a′**

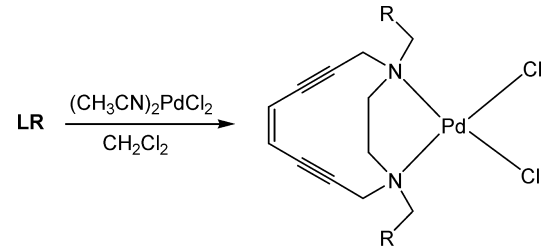

4

R		
Ph	$Pd(LPh)Cl_2$,	**4a**
Me	$Pd(LMe)Cl_2$,	**4a'**

Scheme 5. Syntheses of Pd(II) Enediyne Dihalide Complexes **4**−**4c**

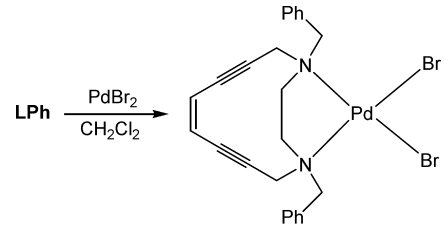

$Pd(LPh)Br_2$, **4b**

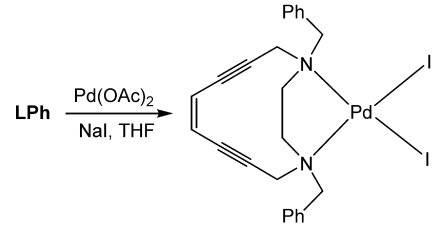

$Pd(LPh)I_2$, **4c**

This produced initial orientation matrices determined from 312 reflections. The data collection was carried out using Mo Kα radiation (graphite monochromator) with a frame time of 5 s and a detector distance of 4.997 cm. A randomly oriented region of reciprocal space was surveyed to the extent of 1.3 hemispheres and to a resolution of 0.553 Å. Three major sections of frames were collected with 0.30° steps in ω at three different φ settings and a detector position of −43° in 2θ. An additional set of 50 frames was collected in order to model decay.

The structures were solved using SIR-92[13] and refined with SHELXL-97 and SHELXTL-plus v.5.10 (Bruker Analytical X-ray Systems, Madison, WI). A direct-methods solution was calculated which provided all non-hydrogen atoms from the E-map. Full-matrix least-squares/difference Fourier cycles were performed using data to a resolution of 0.620 Å. All non-hydrogen atoms were refined with anisotropic displacement parameters. The hydrogen atoms were placed in ideal positions and refined as riding atoms with individual isotropic displacement parameters.

In the case of **2a′**, two molecules are present in the asymmetric unit. The structure was found as proposed with two independent molecules per asymmetric unit. The structure is racemically twinned (ratio 54:46). Nonbonding distances of interest are listed in Table

(13) Altomare, A.; Cascarno, G.; Giacovazzo, C.; Gualardi, A. *J. Appl. Crystallogr.* **1993**, *26*, 343–350.
(14) *SHELXTL-plus*, v. 5.10; Bruker Analytical X-ray Systems: Madison, WI.

Table 2. Crystallographic Data for **2a′**, **2b**, **3b**, **3c′**, and **3d**

	2a′	**2b**	**3b**	**3c′**	**3d**
empirical formula	$C_{14}H_{20}N_2Cl_2Cu$	$C_{24}H_{24}N_2Br_2Cu$	$C_{24}H_{24}N_2Br_2Zn$	$C_{24}H_{24}N_2Br_2Zn$	$C_{24}H_{25}I_3N_2Zn$
fw	350.76	563.81	565.64	535.49	787.53
color of crystal	blue	brown	colorless	colorless	colorless
cryst syst	monoclinic	orthorhombic	monoclinic	orthorhombic	orthorhombic
space group	$P2_1$	*Pbca*	*Cc*	$P2_12_12_1$	*Pccn*
a, Å	7.7510(4)	13.8998(8)	19.5612(19)	7.6823(11)	24.3082(10)
b, Å	18.8432(9)	16.8890(9)	16.4082(19)	11.6397(16)	13.9342(6)
c, Å	10.3886(5)	19.2726(10)	7.1526(8)	19.385(3)	17.2305(7)
α, deg					
β, deg	96.7566(13)		99.610(4)		
γ, deg					
V, Å^3	1506.76(13)	4524.3(4)	2263.5(4)	1733.4(4)	5836.2(4)
Z	4	8	4	4	8
ρ_{calcd}, g/cm^3	1.546	1.655	1.660	2.052	1.793
T, K	133(2)	128(2)	120(2)	120(2)	120(2)
λ, Å	0.71073	0.71073	0.71073	0.71073	0.71073
Goodness-of-fit[a] on F^2	1.047	1.011	1.003	1.073	1.033
final *R* indices $[I > 2\sigma(I)]$[b]	R1 = 0.0250,	R1 = 0.0292,	R1 = 0.0288	R1 = 0.0442	R1 = 0.0257
	wR2 = 0.0559	wR2 = 0.0644	wR2 = 0.0613	wR2 = 0.1054	wR2 = 0.0545
R indices[c] (all data)	R1 = 0.0284,	R1 = 0.0495,	R1 = 0.0342	R1 = 0.0514	R1 = 0.0376
	wR2 = 0.0573	wR2 = 0.0728	wR2 = 0.0634	wR2 = 0.1093	wR2 = 0.0571
largest diff. peak and hole	0.341 and −0.335 *e*•Å^{-3}	0.772 and −0.568 *e*•Å^{-3}	0.705 and −0.370 *e*•Å^{-3}	3.250 and −0.742 *e*•Å^{-3}	0.866 and −0.520 *e*•Å^{-3}

[a] Goodness-of-fit = $[\sum[w(F_o^2 - F_c^2)^2]/N_{observns} - N_{params})]^{1/2}$, all data. [b] R1 = $\sum(|F_o| - |F_c|)/\sum|F_o|$. [c] wR2 = $[\sum[w(F_o^2 - F_c^2)^2]/\sum[w(F_o^2)^2]]^{1/2}$.

Table 3. Crystallographic Data for **4a**•1.75CH_2Cl_2, **4b**•1.75CH_2Cl_2, and **4c**

	4a•1.75CH_2Cl_2	**4b**•1.75CH_2Cl_2	**4c**
empirical formula	$C_{25.75}H_{27.50}N_2Cl_{5.50}Pd$	$C_{25.75}H_{27.50}N_2$ $Br_2Cl_{3.50}Pd$	$C_{24}H_{24}N_2I_2Pd$
fw	666.37	755.29	700.05
color of crystal	yellow	yellow	red
cryst syst	monoclinic	triclinic	orthorhombic
space group	$P2_1/c$	$P\bar{1}$	*Pbca*
a, Å	16.9772(7)	13.777(2)	14.331(3)
b, Å	14.0789(6)	14.187(2)	17.260(4)
c, Å	23.4458(9)	15.996(3)	19.095(4)
α, deg		79.305(4)	
β, deg	99.8500(10)	68.919(4)	
γ, deg		75.504(6)	
V, Å^3	5521.4(4)	2808.6(8)	4723.2(4)
Z	8	4	8
ρ_{calcd}, g/cm^3	1.603	1.786	1.971
T, K	120(2)	140(2)	136(2)
λ, Å	0.71073	0.71073	0.71073
goodness-of-fit[a] on F^2	1.026	0.993	1.047
Final *R* indices $[I > 2\sigma(I)]$[b]	R1 = 0.0321	R1 = 0.0726	R1 = 0.0209
	wR2 = 0.0741	wR2 = 0.1784	wR2 = 0.0455
R indices[c] (all data)	R1 = 0.0459	R1 = 0.1270	R1 = 0.0297
	wR2 = 0.0804	wR2 = 0.2085	wR2 = 0.0498
largest diff. peak and hole	0.927 and −0.731 *e*•Å^{-3}	2.095 and −3.205 *e*•Å^{-3}	1.157 and −0.465 *e*•Å^{-3}

[a] Goodness-of-fit = $[\sum[w(F_o^2 - F_c^2)^2]/N_{observns} - N_{params})]^{1/2}$, all data. [b] R1 = $\sum(|F_o| - |F_c|)/\sum|F_o|$. [c] wR2 = $[\sum[w(F_o^2 - F_c^2)^2]/\sum[w(F_o^2)^2]]^{1/2}$.

1. A least-squares fit of the independent molecules (named molecules A and B) is included.

In the case of **3c′**, the space group $P2_12_12_1$ was determined on the basis of intensity statistics and systematic absences. A direct-methods solution was calculated which provided most non-hydrogen atoms from the E-map. Full-matrix least-squares/difference Fourier cycles were performed, which located the remaining non-hydrogen atoms. All non-hydrogen atoms were refined with anisotropic displacement parameters. The hydrogen atoms were placed in ideal positions and refined as riding atoms with relative isotropic displacement parameters. The final full-matrix least-squares refinement converged to R1 = 0.0442 and wR2 = 0.1093 (F^2, all data). The remaining electron density is rather high. The highest peaks are located around the iodine atoms at an average distance of 1 Å. The possibility of disorder was considered but proved to be not chemically sensible. An attempt to correct the data for twinning by omitting reflections overlapped with the second major component did not result in a better refinement or decrease residual electron density. The remaining peaks are attributed to irresolvable, random twinning of more than two components, which would also explain streaks in reciprocal space. No voids were found in the structure as determined by PLATON.[15]

In the case of **3d**, the hydrogen atoms were placed in ideal positions and refined as riding atoms with relative isotropic displacement parameters. The exception was the H atom at N2, which was found in the difference map and for which an isotropic displacement parameter was refined. Remaining electron density indicated that solvent was present in the structure. The pattern fitted one hexane molecule superimposed with at least two positions for a dichloromethane molecule, which additionally were disordered

(15) Spek, A. L. *Acta Crystallogr.* **1990**, *A46*, C34.

Table 4. Selected Bond Lengths (Å) and Angles (deg) of **3b**, **3c′**, and **3d**

3b		**3c′**		**3d**	
		Distances			
Br1−Zn1	2.3782(5)	I1−Zn1	2.5564(12)	I1−Zn1	2.5806(4)
Br2−Zn1	2.3265(4)	I2−Zn1	2.5774(12)	I2−Zn1	2.5977(4)
Zn1−N1	2.110(3)	Zn1−N1	2.128(8)	I3−Zn1	2.5779(4)
Zn1−N2	2.127(2)	Zn1−N2	2.109(8)	Zn1−N1	2.182(3)
C2−C3	1.194(4)	C2−C3	1.182(16)	C2−C3	1.191(5)
C4−C5	1.326(5)	C4−C5	1.368(19)	C4−C5	1.343(5)
C6−C7	1.190(4)	C6−C7	1.186(15)	C6−C7	1.189(5)
		Angles			
N1−Zn1−N2	89.40(9)	N1−Zn1−N2	86.8(3)	N1−Zn1−I3	105.67(7)
N1−Zn1−Br2	118.57(6)	N1−Zn1−I2	110.8(2)	N1−Zn1−I1	108.36(7)
N2−Zn1−Br2	119.16(7)	N2−Zn1−I2	111.0(2)	I3−Zn1−I1	112.791(16)
N1−Zn1−Br1	106.66(6)	N1−Zn1−I1	120.2(2)	N1−Zn1−I2	105.66(7)
N2−Zn1−Br1	108.70(7)	N2−Zn1−I1	120.5(2)	I3−Zn1−I2	114.013(14)
Br2−Zn1−Br1	111.913(17)	I2−Zn1−I1	106.57(4)	I1−Zn1−I2	109.862(14)

Table 5. Selected Bond Lengths (Å) and Angles (deg) of **4a**·1.75 CH_2Cl_2, **4b**·1.75 CH_2Cl_2, and **4c**

	4a	**4b**	**4c**	
		Distances		
Pd1A−N1A	2.081(2)	2.100(8)	2.143(2)	Pd1−N1
Pd1A−N2A	2.099(2)	2.126(7)	2.143(2)	Pd1−N2
Pd1A−Cl1A	2.3109(7)		2.5850(5)	Pd1−I1
Pd1A−Cl2A	2.3132(7)		2.6020(4)	Pd1−I2
Pd1A−Br2A		2.4235(13)		
Pd1A−Br1A		2.4374(11)		
C2A−C3A	1.193(4)	1.205(15)	1.195(4)	C2−C3
C4A−C5A	1.336(5)	1.323(16)	1.352(4)	C4−C5
C6A−C7A	1.192(4)	1.200(16)	1.192(4)	C6−C7
		Angles		
N1A−Pd1A−N2A	85.70(9)	85.7(3)	84.75(8)	N2−Pd1−N1
N1A−Pd1A−Cl1A	91.87(6)		175.28(6)	N2−Pd1−I1
N2A−Pd1A−Cl1A	175.19(7)		93.86(6)	N1−Pd1−I1
N1A−Pd1A−Cl2A	176.36(6)		93.24(6)	N2−Pd1−I2
N2A−Pd1A−Cl2A	90.99(6)		175.58(6)	N1−Pd1−I2
Cl1A−Pd1A−Cl2A	91.53(2)		88.453(14)	I1−Pd1−I2
N1A−Pd1A−Br1A		92.9(2)		
N2A−Pd1A−Br1A		175.9(2)		
Br2A−Pd1A−Br1A		90.41(4)		
N1A−Pd1A−Br2A		176.5(2)		
N2A−Pd1A−Br2A		91.1(2)		

over an inversion center. However, such a model refined with a strong set of restraints and constraints did not converge to a chemically sensible structure. Therefore, the structure was investigated for solvent-accessible areas.[15] Four voids were found (914.5 Å^3 per unit cell) to contain 135 electrons. For comparison, dichloromethane occupies ca. 78 Å^3 with 42 electrons and hexane occupies 107 Å^3 with 42 electrons.[16] The contribution of the unidentified solvent to the structure factors was assessed by back-Fourier transformation, and the data were corrected accordingly. The refinement using the modified data set improved the overall structure and R1 by about 3%. The final full-matrix least-squares refinement converged to R1 = 0.0257 and wR2 = 0.0571 (F^2, all data). The remaining electron density is located in the vicinity of the iodine atoms.

In the cases of **4a** and **4b**, the structure was found with two Pd complexes and 3.5 dichloromethane molecules per asymmetric unit. The complexes pack very inefficiently, creating voids, which are filled with solvent. One dichloromethane molecule in **4a** is disordered over an inversion center (0, 1/2, 1/2).

(16) Immrizi, A.; Perini, B. *Acta Crystallogr.* **1977**, *A33*, 216–218.

Results and Discussion

Syntheses. Ligand 1,4-diethyl-1,4-diaza-cyclododec-8-ene-6,10-diyne (R = phenyl, **1a′**) is prepared by an analogous procedure to that of 1,4-phenyl-1,4-diaza-cyclododec-8-ene-6,10-diyne (R = phenyl) **1a**.[9] Briefly, reaction of 1,8-dibromooct-4-ene-2,6-diyne[17] with N,N′-diethylethylenediamine in the presence of K_2CO_3 in N,N-dimethylformamide at 0 °C produces **1a′** in 20% isolated yield (Scheme 1) with a concomitant generation of insoluble polymeric materials. Complexation of **1** with $CuCl_2 \cdot 2H_2O$ and $CuBr_2$ in MeOH/CH_2Cl_2 (1:1) at room temperature generates the corresponding copper metalloenediyne dichloride (**2a**, **2a′**) and dibromide (**2b**) complexes (∼90% yield) as green and dark red solids, respectively (Scheme 2). The colorless d^{10} $ZnLRX_2$ (R = Ph, **3a**−**3c**; R = Me, **3a′**−**3c′**) compounds were synthesized in the same manner using ZnX_2 (X = Cl, Br, I) as the divalent metal ion source (71%; Scheme 3). During crystallization (∼72 h), the zinc diiodide compound **3c** decomposes in CH_2Cl_2 to produce the $[ZnI_3^-][HLPh^+]$ ion pair **3d**. Although a variant of the desired species, the crystal structure and solid-state reactivity (evaluated from single crystals) serve as valuable benchmarks for the thermal reactivities of the title compounds (*vide infra*).

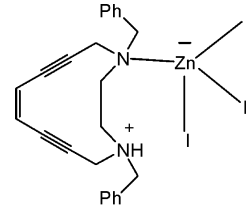

3d

Reaction of **1** with $(CH_3CN)_2PdCl_2$ in CH_2Cl_2 at room temperature for 2 h produces the corresponding $PdLRCl_2$ compounds (**4a**, **4a′**) in ∼70% yield (Scheme 4). Analogously, $PdLPhCl_2$ compound **4b** is formed by reacting **1a** with $PdBr_2$, while the purple $PdLPhI_2$ species **4c** is obtained in 40% yield by refluxing **1a** with palladium acetate in dry THF in the presence of excess sodium iodide under nitrogen for 24 h (Scheme 5).

(17) Rawat, D. S.; Zaleski, J. M. *Syn. Commun.* **2002**, *32* (10), 1489–1494.

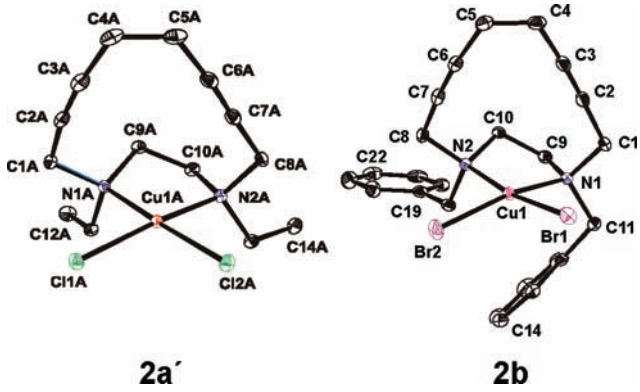

Figure 1. X-ray structures and atom labeling scheme for **2a′** and **2b**. Thermal ellipsoids are illustrated at 40% probability.

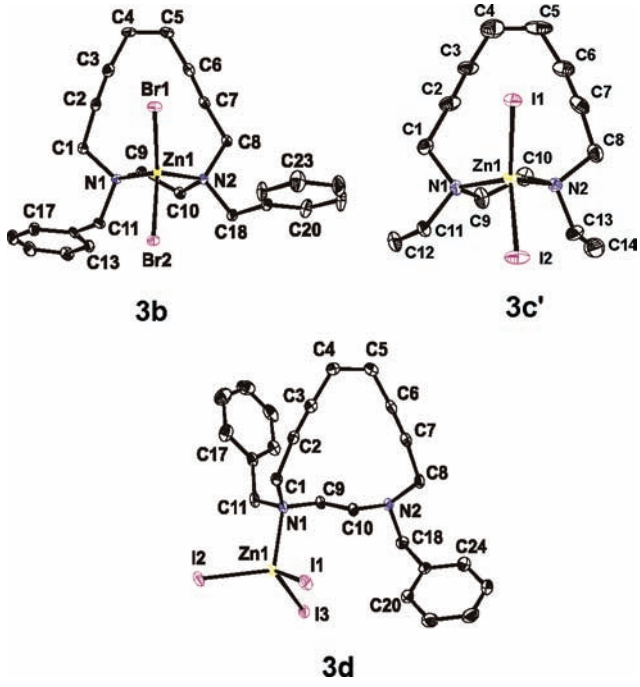

Figure 2. X-ray structures and atom labeling scheme for **3**, **3c′**, and **3d**. Thermal ellipsoids are illustrated at 40% probability.

X-Ray Structures of 2−5. The X-ray crystallographic data for **2a′**, **2b**, **3b**, **3c′**, and **3d** are given in Table 2, and those of **4a**−**4c** in Table 3, with selected bond lengths and angles in Tables 1, 4, and 5. All single crystals were obtained by the slow diffusion of dichloromethane solution into hexane at 0 °C. ORTEP plots of **2a′** and **2b** (Figure 1); **3b**, **3c′**, and **3d** (Figure 2); and **4a**−**4c** (Figure 3) are shown at 40% probability.

The structures of **1a′** (not shown) and **1a**[9] reveal a conformationally strained enediyne unit that bridges an ethylenediamine chelate in the *anti* configuration. More subtly, the ethylene bridge between the chelating tertiary amines constrains the enediyne fragment so that the critical distance and enediyne conformation are almost independent of the local geometry of the metal center. This is unlike

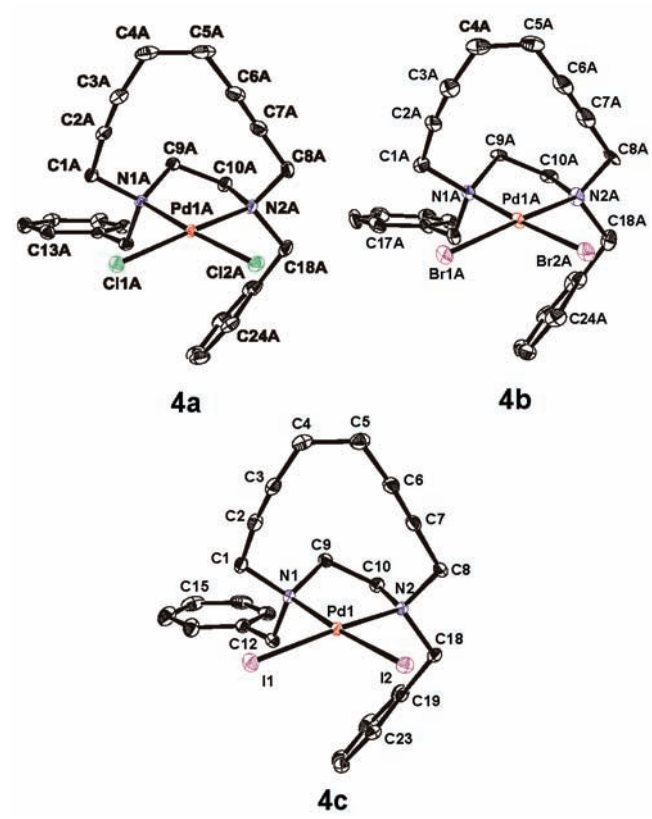

Figure 3. X-ray structures and atom labeling scheme for **4a**−**4c**. Thermal ellipsoids are illustrated at 40% probability.

previous acyclic enediyne ligating constructs that revealed stark reactivity dependencies based on metal center geometry.[12,18,19]

The X-ray crystal structures of **2**−**4** are insightful as only a limited number of enediyne ligands and their corresponding metalloenediyne complexes have been crystallographically characterized.[20−25] The metal center geometries of metalloenediynes **2**−**4** (**2**, distorted square planar; **3**, tetrahedral; **4**, square planar) are as expected for these d^9, d^{10}, and d^8 metalloenediynes, respectively. These complexes also exhibit *cis*-MN_2Cl_2 stereochemistry, indicating that the metalloenediynes must undergo a low-barrier conformational change prior to chelation.

The $Cu(LPh)Cl_2$ compound **2a**[9] exhibits a *syn* conformation of the ethylenediamine unit and a slightly distorted square-planar geometry of the copper center common to four-coordinate *cis*-CuN_2Cl_2 structures.[12] Similarly, for the more rigorously square-planar complex **2a′** (R = Me; X = Cl), the syn conformation of the tightly chelated nitrogens (∼2.08

(18) Rawat, D. S.; Zaleski, J. M. *J. Am. Chem. Soc.* **2001**, *123*, 9675–9676.

(19) Rawat, D. S.; Benites, P. J.; Incarvito, C. D.; Rheingold, A. L.; Zaleski, J. M. *Inorg. Chem.* **2001**, *40*, 1846–1857.

(20) Kawano, T.; Kuwana, J.; Du, C.-X.; Ueda, I. *Inorg. Chem.* **2002**, *41*, 4078.

(21) Hu, Y.-Z.; Chamchoumis, C.; Grebowicz, J. S.; Thummel, R. *Inorg. Chem.* **2002**, *41*, 2296.

(22) Chandra, T.; Pink, M.; Zaleski, J. M. *Inorg. Chem.* **2001**, *40*, 5878–5885.

(23) Bosch, E.; Barnes, C. L. *Inorg. Chem.* **2001**, *40*, 3097.

(24) Schmitt, E. W.; Huffman, J. C.; Zaleski, J. M. *Chem. Commun.* **2001**, 167–168.

(25) Coalter, N. L.; Concolino, T. E.; Streib, W. E.; Hughes, C. G.; Rheingold, A. L.; Zaleski, J. M. *J. Am. Chem. Soc.* **2000**, *122*, 3112–3117.

Å) causes strain in the ethylenediamine unit, leading to a moderate compression of the alkyne termini separation (C2···C7) from ∼3.90 Å[9] for the free ligand(s) to ∼3.75 Å (3.74 Å for **2a′**; 3.76 Å for **2a**). The N1−Cu−N2 and Cl1−Cu−Cl2 angles in **2a′** are nearly idealized (90°), with the former adopting only a slightly reduced bite angle (∼86°). In the case of **2b** (R = Me; X = Br), the metal center geometry is almost identical to **2a**, but the alkyne termini separation (C2···C7) is slightly larger (3.88 Å), which is caused by a general increase of all ligand bond lengths at the copper center (Table 1).

The Zn(II) analogues **3** (Figure 2) possess structural commonalities but also significant differences with respect to their Cu(II) counterparts. The d^{10} electronic configuration results in a tetrahedral disposition of the ligands about the *cis*-ZnN_2X_2 core. While the Zn−N bond distances increase to ∼2.12 Å relative to the Cu(II) family, the N1−Zn−N2 bond angle increases only slightly, reflecting a similar conformation restriction by the bridging ethylene unit. In contrast, the X1−Zn−X2 angles (∼110−112°) are expanded to and slightly beyond that expected for a tetrahedral structure. In general, compounds **3a** and **3b** are isostructural, with nearly identical (3.75 Å) alkyne termini separations. Variation in the steric bulk of the ligand and donating halogen (*i.e.*, Zn(LMe)I_2, **3c′**), leads to only a small increase in alkyne termini separation (3.82 Å) over **3a**−**3b**. The only important structural difference is manifested in their Zn−X bond lengths; the Zn−Br bond in **3b** is 0.16 Å longer than Zn−Cl bond in **3a**.

The structure of **3d** (Figure 2) is intriguing, as it reveals a [ZnI_3^-][$HLPh^+$] ion pair likely deriving from protonation of the amine by residual water, and consequential incorporation of an additional I^- into the Zn(II) coordination sphere for charge balance. With only one nitrogen donor coordinated to Zn(II), the enediyne ligand adopts the same *anti* conformation observed in the free ligand structures **1a** and **1a′**. This also leads to an alkyne termini separation (3.97 Å) reminiscent of the larger distances of the free ligands **3a** or **3b** (∼3.75 Å).

The d^8 configuration of the Pd(II) derivatives **4a**−**4c** produces square-planar *cis*-PdN_2Cl_2 complexes (Figure 3) that structurally parallel their Cu(II) counterparts, but with elongated Pd−N and Pd−X bond lengths (Table 5). The conformation of the enediyne ligand is retained, but the increased Pd−N bond lengths increase the alkyne termini separation slightly (3.82−3.88 Å) to a distance between the Cu(II) complexes (∼3.75 Å) and the free ligand **1a** (3.90 Å). The Pd−X bond length also increases gradually down the halogen group from 2.31 Å for **4a** (X = Cl) to 2.59 Å for **4c** (X = I).

Overall, despite the significant differences in the metal coordination geometry for Cu(II), Zn(II), and Pd(II), which in unrestricted enediyne ligands leads to dramatic differences in critical distance, the ethylene bridge maintains the same conformation of the bound enediyne ligand with only a modest variation in the alkyne termini separation.

Scheme 6. Bergman Cyclization of **2**−**4** in the solid state

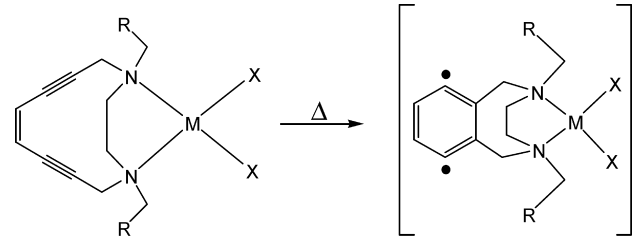

2 - 4

Table 6. Solid-State Bergman Cyclization Temperatures of **1**−**5** Determined by DSC

compounds	cyclization temperatures/°C	alkyne termini separation/Å
LPh (**1a**)	170	3.90
LMe (**1a′**)	168	
Cu(LPh)Cl_2 (**2a**)	141	3.76
Cu(LMe)Cl_2 (**2a′**)	136	3.74
Cu(LPh)Br_2 (**2b**)	148	3.88
Zn(LPh)Cl_2 (**3a**)	207	3.75
Zn(LPh)Br_2 (**3b**)	154	3.74
Zn(LPh)I_2 (**3c**)	144	
Zn(LMe)Cl_2 (**3a′**)	194	
Zn(LMe)Br_2 (**3b′**)	200	
Zn(LMe)I_2 (**3c′**)	196	3.82
Zn(LPhH)I_3 (**3d**)	199	3.97
Pd(LPh)Cl_2 (**4a**)	225	3.82
Pd(LMe)Cl_2 (**4a′**)	207	
Pd(LPh)Br_2 (**4b**)	212	3.88
Pd(LPh)I_2 (**4c**)	196	3.86

Thermal Bergman Cyclization of 1−5. i. Solid-State Reactivity. The solid-state thermal Bergman cyclization reactivities of **1** and the corresponding metalloenediynes **2**−**4** (Scheme 6) have been evaluated by DSC and are given in Table 6. Typically, changes of state due to melting are observed as endotherms, while reactions leading to overall exothermic product formation are observed as exotherms by DSC, even though transition states en route to a product may be endothermic. Within this framework, ligands **1a** and **1a′** show melting endotherms at 70 and 50 °C, respectively, that are followed by a large, irreversible exothermic transition corresponding to the cyclization reaction in the melt (**1a**, 168 °C; **1a′**, 170 °C). For metalloenediynes **2**−**4**, heating of solid samples results in only large, irreversible exothermic peaks which are observed between 140−230 °C, indicating *solid-state* cyclization reactivity, without the melting endotherms observed for ligands **1a** and **1a′**.

In the case of dichloride complexes, the Bergman cyclization temperatures gradually increase from Cu(II) to Pd(II); the cyclization temperatures of **2a**, **3a**, and **4a** are 141 °C, 207 °C, and 225 °C, respectively. The corresponding complexes (**2a′**, **3a′**, and **4a′**) with ligand **1a′** follow the same trend. For the Zn(II) and Pd(II) complexes, the cyclization reaction temperatures gradually reveal a dependence on the ancillary halide ligands (Cl, Br, I). Interestingly, along the series from $ZnCl_2$ to ZnI_2 (**3a**−**3c**), the cyclization temperatures show a marked decrease from 207 to 144 °C, while Pd(II) complexes (**4a**−**4c**) reveal a similar trend, but with a

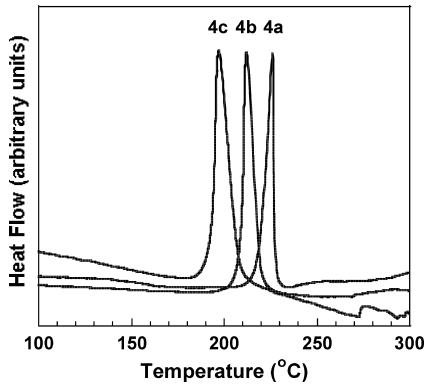

Figure 4. Differential scanning calorimetry traces for the thermal cyclization of **4a**−**4c** in the solid state.

Scheme 7. Bergman Cyclization of **1** to **2** in Solution

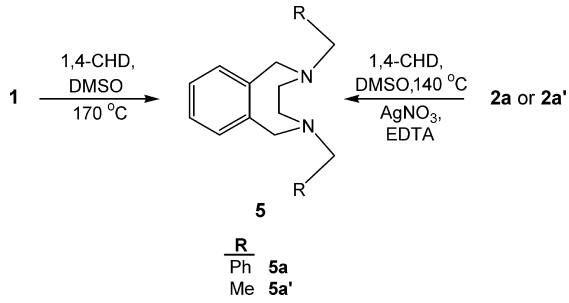

reduced temperature range (225 to 195 °C; Figure 4). In contrast, the cyclization temperatures of Cu(II) complexes **2a** and **2b** are almost unchanged with variation in the halogen ancillary ligands.

ii. Reactivity in Solution. Bergman cyclization reactivities have also been evaluated by product isolation studies in solution for ligands (**1a** and **1a′**) and Cu(II) complexes (**2a** and **2a′**). Heating of **1** in a DMSO solution with 100-fold excess 1,4-cyclohexadiene (CHD) for 10 to 12 h at 170 °C yields Bergman cyclized product **5** in 60−70% yield (Scheme 7). In contrast, heating of the ligands at 140 °C for 10 h under the same conditions leads to no reaction and recovery of only the starting material.

Heating of **2** (**2a** and **2a′**) in a DMSO/CHD solution for 6 h at 140 °C followed by demetalation with $AgNO_3$ and excess EDTA results in generation of Bergman cyclized product **5** in ∼25% isolated yield (Scheme 6). The remaining mass balance consists of insoluble polymeric and decomposition products, without persistence of unreacted starting material. Compounds **5a** and **5a′** were characterized by NMR, mass, and elemental analyses. The most diagnostic feature of cyclized product formation relative to the uncyclized ligands **1a** and **1a′** are the two alkyne resonances (e.g., ^{13}C for **1a′**: δ 83.76 and δ 93.53 ppm) which disappear upon cyclization with a concomitant appearance of two new resonances in the aromatic region.

Chelation of **1** to Cu(II) results in a decrease in the alkyne termini separation by 0.14 Å relative to the free ligand **1**, and thus a corresponding decrease in the cyclization temperature by 29 °C. This observation is consistent with the documented ability of metals to reduce the barrier to enediyne cyclization by reduction of the alkyne termini distance upon chelation. Although this relationship clearly holds for complexes dominated by geometric contributions to enediyne cyclization (i.e., an unrestricted enediyne ligand chelated to a given metal center possessing variable geometries dependent upon the electronic configuration of the metal),[19,24,25] a comparison of metalloenediyne compounds containing a range of metals with different electronic structures has not been described. The importance of an electronic contribution to metalloenediyne reactivity is apparent by comparison of the cyclization temperatures for **2a** and **3a** or **2a′** and **3a′**. Although the Cu(II) and Zn(II) centers possess widely differing coordination geometries, the alkyne termini separation distances in these structures are nearly identical. However, their Bergman cyclization temperatures vary by over 60 °C. Similarly, the Pd(II) compound **4a** has a comparable coordination geometry to **2a** and exhibits only a modest increase in the alkyne termini separation due to the increased metal−ligand bond lengths, yet the Bergman cyclization temperature is over 80 °C greater for **4a**. Geometric effects could play a minor role in the cyclization temperature differences between **2a** and **4a**, but alkyne termini separation in these restricted enediynes clearly cannot be the origin of these observations. Moreover, any contribution from steric differences associated with the chloride ligands in the cyclized product can also be ruled out, as **2a** and **4a** should have nearly identical product geometries, while **3a** and **4a** have very different geometries, yet these compounds exhibit only an 18 °C difference in their cyclization temperatures.

iii. Metal Geometry/Halogen Dependence. In the case of $ZnLPhX_2$ compounds, the geometry places one of the ancillary chloride ligands (Cl1) to within 3.0−3.26 Å of the plane of the diyne unit (Figure 5). This allows the halogen lone pair interaction (through space) to electronically influence Bergman cyclization, as the ligand is spatially proximal to the developing bond between the C2 and C7 carbons. First principles suggests that the addition of electronic density to the developing bond would increase the energy of the transition state due to electron repulsion and therefore increase the activation temperature for the cyclization reaction. It has been observed that cyclization temperatures gradually decreases down the halide series (Cl, Br, I) for Zn(II) compounds **3a**−**3c**. This would be in accordance with the increasing distance between the halogen lone pair and C2···C7 bond. However, in the case of $ZnLMeX_2$ compounds (**3a′**−**3c′**), the Bergman cyclization temperatures are all high and almost identical, revealing no distinct halogen dependence. The high base temperatures (∼195 °C) relative to the Cu(II) series or the $ZnLPhCl_2$ compound indicate that indeed an electron repulsion interaction persists; however, the unusual trend in cyclization temperature of the $ZnLPhX_2$ compounds versus their $ZnLMeX_2$ counterparts as a function of halogen must be at least partially ascribed to the presence of a steric interaction between the large halogen atom and the phenyl ring of the ligand in the transition state. Additionally, the comparable cyclization temperature of compound **3d** (199 °C) is an important control because it reveals

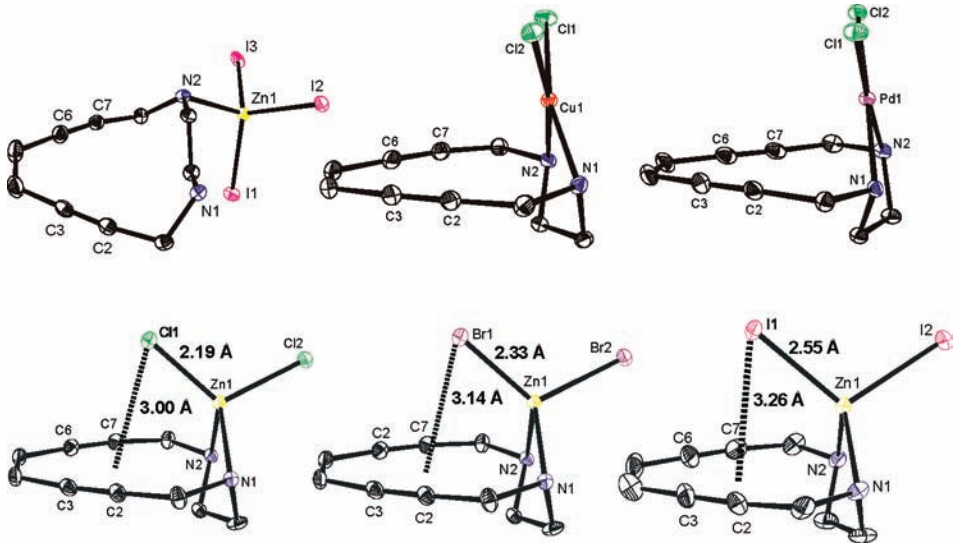

Figure 5. Orientation of chloride ligands in **2a**−**4a** relative to the developing C2···C7 bond.

that cyclization of these ethylenediamine systems is not controlled by chelation-induced alkyne termini reduction, but rather more complex and subtle geometric and electronic effects involving ancillary functionalities.

For the Pd(II) analogues, the increase in cyclization temperature with an increase in Pd−X distance parallels the trend in reactivity observed for the Zn(II) compounds with R = Ph. The square-planar geometry, however, precludes through-space lone pair donation into the enediyne π system but may facilitate through-bond halide lone pair donation to the Pd d orbitals. By analogy to the Zn(II) trend, this donation would decrease as the M−X distance increases, which correlates with the cyclization temperature gradually decreasing on going from chloro- to iodo-substitution, albeit within a less dramatic temperature range. Once again, substitution of **LPh** with **LMe** does show a convoluted contribution to the reaction coordinate from a steric interaction with the phenyl ring. Finally, for the distorted square-planar geometry of the Cu(II) systems, the disposition of halide ligands are such that their lone pairs are likely fully localized, exhibiting neither through-space nor through-bond interactions with the enediyne π system. Thus, variation in the halide ligands in the case of Cu(II) compounds does not influence the overall Bergman cyclization barrier.

Conclusion

A series of ethylenediamine−enediynes has been prepared that isolates the geometric contributions to Bergman cyclization activation energies deriving from metal-induced ligand conformational changes. These scaffolds have allowed an investigation of more subtle electronic effects due to ancillary metal ligands, and steric interactions with ligand substituents. In the presence of metal-mediated enediyne ligand structure change (i.e., alkyne termini separation variations), these effects would likely be masked, and only in a controlled series of compounds are they definable. Two trends are clear from the thermal reactivities of these constructs: the electronic contributions of ancillary ligands or potentially even intraligand functionalities can markedly affect thermal reaction barriers via electron repulsion, and steric interactions along the cyclization reaction coordinate may be important in the observed reaction temperatures. Together, these chemical parameters can have a marked impact on the Bergman cyclization reaction chemistry.

Acknowledgment. The generous support of the National Institutes of Health (R01 GM62541-01A1) is gratefully acknowledged.

Supporting Information Available: CIF files. This material is available free of charge via the Internet at http://pubs.acs.org.

IC801116Q